Front. Earth Sci. 2021, 15(3): 692–704
https://doi.org/10.1007/s11707-021-0897-6

RESEARCH ARTICLE

Uncertainty analysis and visualization of geological subsurface and its application in metro station construction

Weisheng HOU (✉)[1,2,3], Qiaochu YANG[4,1], Xiuwen CHEN[1], Fan XIAO[1,2,3], Yonghua CHEN[5]

1 School of Earth Sciences and Engineering, Sun Yat-sen University, Guangzhou 510275, China
2 Guangdong Provincial Key Lab of Geodynamics and Geohazards, Guangzhou 510275, China
3 Southern Marine Science and Engineering Guangdong Laboratory (Zhuhai), Zhuhai 519080, China
4 Sichuan Highway Planning, Survey, Design and Research Institute Ltd., Chengdu 610041, China
5 Guangzhou Metro Design & Research Institute Co. Ltd., Guangzhou 510010, China

Abstract To visualize and analyze the impact of uncertainty on the geological subsurface, on the term of the geological attribute probabilities (GAP), a vector parameters-based method is presented. Perturbing local data with error distribution, a GAP isosurface suite is first obtained by the Monte Carlo simulation. Several vector parameters including normal vector, curvatures and their entropy are used to measure uncertainties of the isosurface suite. The vector parameters except curvature and curvature entropy are visualized as line features by distributing them over their respective equivalent structure surfaces or concentrating on the initial surface. The curvature and curvature entropy presented with color map to reveal the geometrical variation on the perturbed zone. The multiple-dimensional scaling (MDS) method is used to map GAP isosurfaces to a set of points in low-dimensional space to obtain the total diversity among these equivalent probability surfaces. An example of a bedrock surface structure in a metro station shows that the presented method is applicable to quantitative description and visualization of uncertainties in geological subsurface. MDS plots shows differences of total diversity caused by different error distribution parameters or different distribution types.

Keywords uncertainty, geological sub-surface model, vector parameters, multiple-dimensional scaling

1 Introduction

Three-dimensional geological model is a kind of mathematical model that illustrates the spatial distribution of geological structures or properties in 3D perspective. Similar to 2D geological mapping, a good 3D model also helps geologists understand the geological processes. However, due to sparsity or imprecision of input data and incomplete recognition of geological phenomena, uncertainty inevitably exists in the modeling process and the final modeling result (Bárdossy and Fodor, 2004; Bond et al., 2007; Wellmann et al., 2010; de Kemp et al., 2016; González-Garcia and Jessell, 2016). The qualitative and quantitative description of uncertainties in geological models seriously impacts decision-making in applications in many fields, such as mineral prospecting and oil and gas reservoir appraisal (Thore et al., 2002; Bistacchi et al., 2008; Scheidt et al., 2015; Lee et al., 2016). In the past decade, a number of studies have largely discussed the detection, evaluation, and analysis of uncertainties in 3D geological modeling (e.g., Mann, 1993; Tacher et al., 2006; Caers, 2011; Bond, 2015).

The uncertainty existing in 3D geological model is attributed mainly to three components: imprecise measurements in input data, error generated during the modeling process, and imprecise or unknown information (Mann, 1993; Bárdossy and Fodor, 2004; Wellmann et al., 2010). Uncertainties caused by imprecise information cannot be quantitatively described easily. Error generated during the modeling process is a type of stochastic error that shows up in the process of interpolation of the subsurface or is caused by combining data. Currently, most studies are focusing on quantifying uncertainties caused by imprecise measurements of input data for 3D modeling. Imprecise measurements in input data include measurement errors and imprecise interpretation, such as stratigraphic contact position. Uncertainty caused by imprecise measurements appears as uncertain positions between different lithological boundaries or rock types.

Received October 17, 2020; accepted March 2, 2021

E-mail: houwsh@mail.sysu.edu.cn

Attempting to reduce impacts to the final model, some methods focus on the variability of uncertainty introduced by humans or computation during data collection, processing, and representation (Thore et al., 2002; Jones et al., 2004; Tacher et al., 2006; Lindsay et al., 2012). Some other methods attempt to quantify impacts of errors and uncertainties in final 3D models (Caumon et al., 2009; Jessell et al., 2010; Wellmann et al., 2010; Wellmann and Regenauer-Lieb, 2012). Assuming that errors existing in input data are independent of each other and each type of error is described by a certain distribution, such as a normal distribution or uniform distribution (Wellmann et al., 2010), uncertainties are characterized by measuring a distribution function parameter (such as the standard deviation) at a single-point position. With the variogram or covariance model, geostatistical method explores uncertainty quantitatively and the spatial relationships between sample points (Bárdossy and Fodor, 2004; Tacher et al., 2006). Building a 3D model suite with perturbed input data is an alternative option for uncertainties analysis. Lindsay et al. (2012, 2013) analyzed uncertainty in the final model with a suite of implicit models generated from orientation measurements. Also, geometry uncertainty in 3D model with perturbed input data can be described with a set of geometrical 'geodiversity' metrics (Lindsay et al., 2013). A stochastic downscaling method based on orientation variations of fault is presented to simulate multiple fault surfaces with different topological relations (Julio et al., 2015). When input data and a final 3D model are represented using raster models such as the voxel or grid, geostatistical methods or information entropy-based methods become an effective choice for error or uncertainty analysis on each vertex (Chilès et al., 2004; Calcagno et al., 2008; Guillen et al., 2008; Wellmann et al., 2010; Wellmann and Regenauer-Lieb, 2012).

Scalar parameters that are used to measure uncertainties in the methods mentioned above achieve low-dimension representation of uncertainties. Note that scalar parameter usually is summarized with parametric statistics such as mean value and standard deviation (Hollister, 2015). Many studies have shown that multiple models display overall similar, whereas possibly significant differences in geological architecture maybe exist (Jessell et al., 2010; Wellmann et al., 2010; Lindsay et al., 2012). Naturally, in three-dimensional space, uncertainty in the 3D geological model has high dimensional and anisotropic characteristics. Especially, when multiple 3D geological models are obtained and used to describe spatial uncertainties, parametric statistics show global variations as a whole entity and geometrical measures are difficult to exactly reveal differences of geological elements. A set of geometrical 'geodiversity' metrics including depth, curvature, and geological complexity is proposed as indicators for analyzing uncertainty in structural surface suite (Lindsay et al., 2013). However, some questions remain: Can uncertainties in 3D geological model be characterized by other parameters, such as vector parameters? Which kind of vector parameter(s) is fit for uncertainty measurement? How do these parameters measure and represent uncertainties variation? In this study, some vector parameters including normal vector, curvatures and their entropy are introduced to measure uncertainty in the geological subsurface. To explore vector properties of uncertainty, we reconstruct an isosurface suite with scalar quantitative indicators such as geological attribute probability (GAP, Hou et al., 2019). The vector and geometric parameters are used to represent the geometry of the isosurface. Thus, uncertainties in subsurface are converted into spatial variations of vector and geometric parameters. Perturbed input data with different error distributions and the response of uncertainties presented by parameters for the GAP subsurface suite are discussed with the multiple-dimensional scaling (MDS) method.

2 Methods

2.1 Study area and basic idea

This study is carried out based on fault subsurface at a metro station of Line 11 in the downtown area of Guangzhou city, southern China. According to a previous geological investigation (Guangdong Geological and Mineral Bureau, 1989), the Guangsan Fault lies along the section of Metro Line 11 (Fig. 1). A metro system is a convenient means of public transportation. During the design and construction of a metro system, the 3D distribution of lithologies, strata, and faults forms a basis for assessing aquifer recharge and vulnerability and should be a particular concern (Turner and Kessler, 2015). Faulting changes rock mechanics and may cause geological problems such as water inrush and slope collapse. Therefore, building a 3D fault surface model with boreholes was the first step for analyzing the impact of the fault to the metro design and construction. Here, core samples from 21 boreholes were collected and interpreted to obtain exact stratigraphic information. The fault surfaces revealed by the boreholes were constructed with GOCAD® and smoothed using the Discrete Smoothing Interpolation (DSI) method. The contact positions of fault and strata were not clear because of cracked rock samples. Hence, errors exist in measuring fault positions. Measurement errors will impact and propagate to errors on the fault subsurfaces that we constructed.

A step-wised uncertainty analysis method, in this study, is proposed as shown in Fig. 2. First, a geological model is constructed and used as a best-guess model. Error distribution functions are preset on each sample point. Note that recognizing the contact between two formations in a borehole or outcrop is a tough task. Therefore, selecting error distribution should be carefully carried out

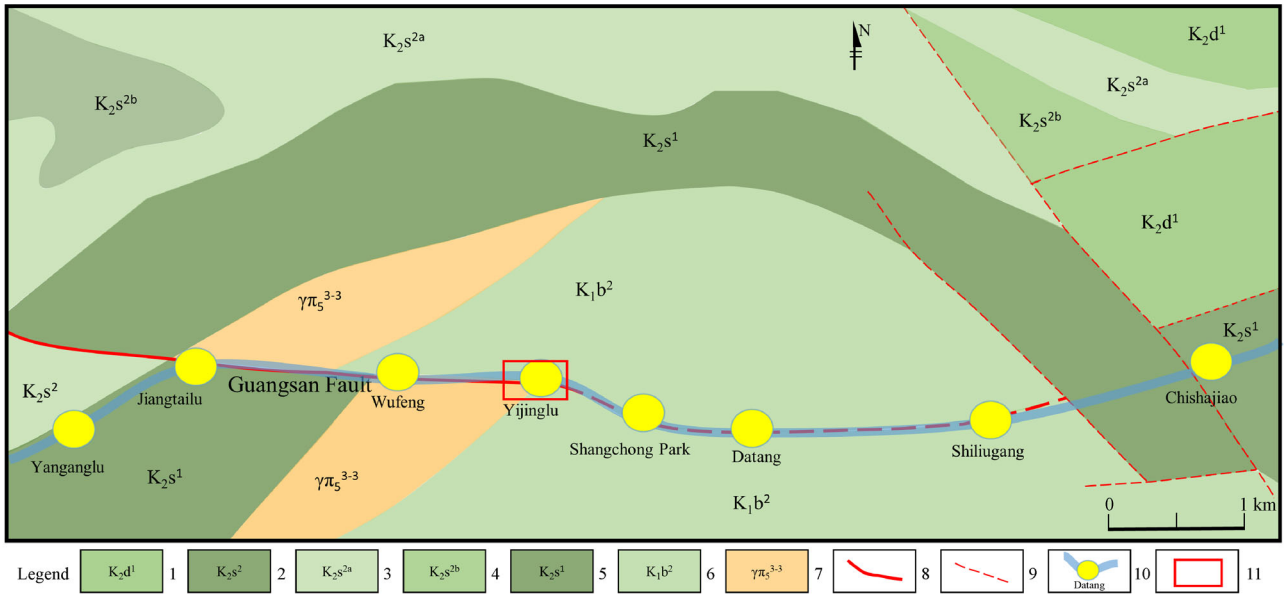

Fig. 1 Bedrock geology map. 1—Lower section of Dalangshan Group of Cretaceous; 2—Upper section of Sanshui Group of Cretaceous; 3—Donghu section of Sanshui Group of Cretaceous; 4—Xihao section of Sanshui Group of Cretaceous; 5—Lower section of Sanshui Group of Cretaceous; 6—Upper section of Baihedong Group of Cretaceous; 7—Subrhyolite; 8—Guangsan Fault; 9—Burried Fault; 10—Metro Line and metro stop; 11—Modeling area.

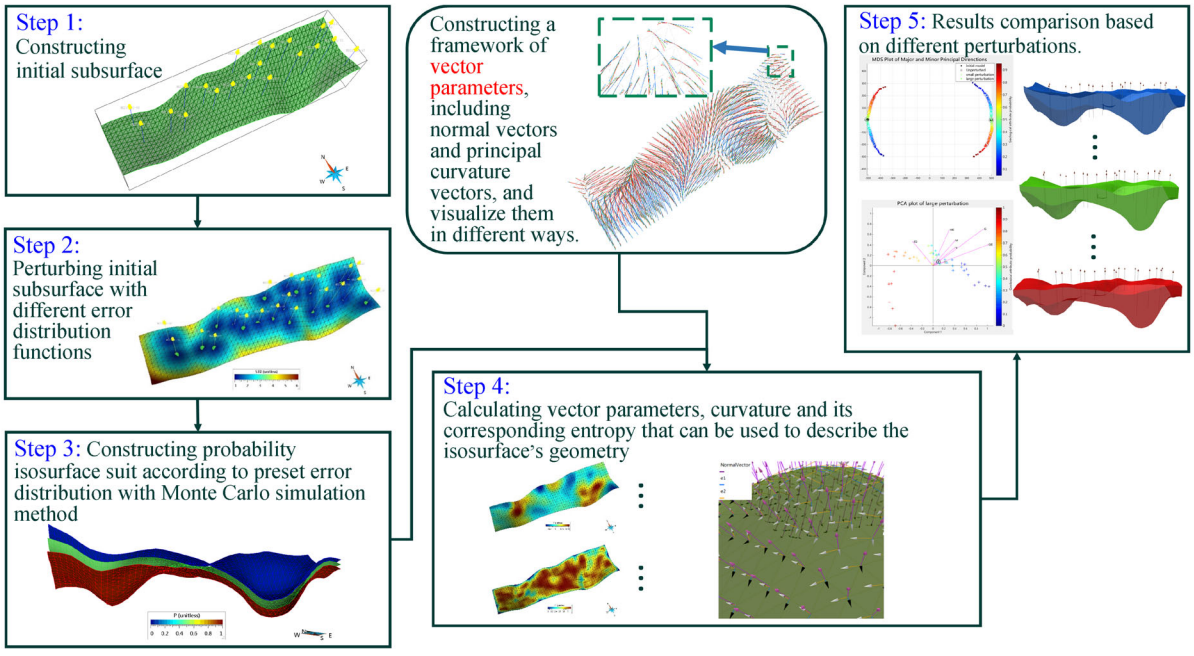

Fig. 2 Flowchart of vector parameters-based uncertainty analysis for 3D geological subsurface.

according the lithology related to the contacts. Here, the error distribution on sample point is preset according to the basic idea presented by Wellmann et al. (2010). On unsampled points, error distribution functions are determined by the error distribution function of the nearest sample point. Then, a model suite is constructed by the Monte Carlo (MC) simulation with error distributions. Simulation results at each point indicate an occurrence of lithology termed with GAP. In fact, the GAP value of each point is an occurrence of a type of attributes appeared. A GAP isosurface suite with error perturbance in input data is constructed to visualize and analyze uncertainty variation

differences. Several types of parameters including normal vector, principal curvature and their entropy are introduced to characterize the variation of isosurface geometry. Finally, geometry variations among different GAP isosurfaces characterized with vector parameters are compared with different methods.

2.2 Geological attribute probability and its isosurface

Any spatial point underground has its own attributes, such as geochemical element components, physical properties, or lithological characteristics. In 3D geological modeling, geological contacts are determined according to attributes of neighboring geological blocks. For example, the geometry of a geological structures is determined by lithology that are correlated to the contact. In essence, geometry uncertainty of subsurface is the uncertainty of geological attributes in 3D space (e.g., Tacher et al., 2006; Wellmann et al., 2010; Hou et al., 2019). The spatial error distribution can be characterized by probability (Tacher et al., 2006), and the probability can be calculated as (Hou et al., 2019):

$$P(A) = F(u) = \int_a^b f(z)\mathrm{d}z, \tag{1}$$

where z is the depth of contact, $f(z)$ is the probability density function, a and b are bounded values of the confidence interval at a chosen level, the cumulative distribution function $P(A)$ is a function of position or z value. Therefore, the error distribution at a point can be transferred into an occurrence of lithology or other geological attributes, which is termed with GAP.

On the sample point, a normal distribution corresponding to a continuous contact and a uniform distribution corresponding to a missing contact are the most typical geological attribute probability density functions (Wellmann et al., 2010; Li et al., 2013). On the unsampled points, errors can be estimated or predicted by variogram model in traditional statistics, based on priori assumption that a single error distribution (Gaussian) exists across all kinds of spatial data. With the terminology of GAP, different kinds of spatial error distribution can be transformed into GAP values and be summed directly with an entropy-based weight method (Hou et al., 2019). In the entropy-weighted method, errors are followed or limited by error distributions of the endpoints, which results in errors on the unsampled points are smaller than the values on the sample points.

However, the error at the unsampled point should be bigger than the error at the sample point. Also, uncertainty on the unsampled points should be greater than uncertainty on the sample points as pointed out by Wellmann et al. (2010). Therefore, in this study, we assumed that:

1) The confidence interval of an unsampled point has positive correlation with the distance of the nearest borehole. It means that the closer to the borehole, the smaller the confidence interval should be at the node.

2) With the increase of the distance between the node and nearest borehole, the parameters of the error distribution function show a nonlinear increasing trend from slow to fast.

3) The standard deviation and the error impact of known points can be adjusted with changing the parameters of the equation.

To describe the characteristics of uncertainties on unsampled points mentioned above, here, a function with standard deviation related to sample points is presented:

$$\sigma(i) = \left[A \times \frac{e^{x_i} - 1}{e - 1} + 1\right]\sigma_{\text{sample min}}(i),$$

$$x_i = d_{\min}(i)/\max(d_{\min}),\ x_i \in [0,1], \tag{2}$$

where $d_{\min}(i)$ is the distance between the ith node on the subsurface network and the nearest sample point and max ($d_{\min}$) is the maximum value of all $d_{\min}$. x_i, termed the "regularized distance", equals 0 when the node is coincident with the sample point, and $x_i = 1$ if the node is the farthest node to the sample point. $\sigma_{\text{sample min}}(i)$ is the standard deviation on the nearest sample point to a current node. When the unsampled point is at the same distance from two sample points, the smaller value of $\sigma_{\text{sample min}}(i)$ is selected. A, termed the "distance factor," is a constant for amplifying the error impact in input data and can be given by any positive number that is larger than 1. The distance factor in fact is a kind of scaling factor to enlarge the extreme value of the confidence interval. It also helps to set discretionarily according to the need of visualization. Therefore, the standard deviation on each point of the subsurface can be obtained. Figure 3 illustrates the variation of standard deviation variation with distance. The left image in Fig. 3 shows three points with different distances to a sample point. The points marked ① and ③ are the farthest and shortest point to their nearest sample point respectively. When all sample points have the same standard deviation value, the standard deviation increases when the distance gets longer, as shown in the right image of the Fig. 3. Figure 4 shows the variation of standard deviation on the surface with different distance factors when the standard deviation is 1.0. The standard deviation is obviously larger on unsampled points than on sample points. Also, the value of standard deviation on the unsampled points increases with distance increase. This means that unsampled points have more uncertainty than the sample points.

2.3 Parameters for uncertainty measurement and its visualization

In this study, several types of vector parameters, including the normal vector and principal curvature, as well as mean

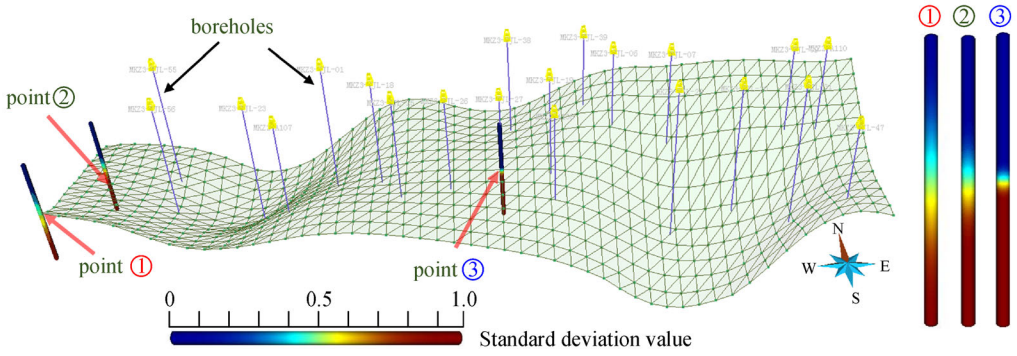

Fig. 3 Standard deviation on different points of the surface network. Points marked with ① and ③ are the longest distance and the shortest distance from the nearest sample point respectively in the left image. The color bars in the right illustrated the standard deviation distribution along the z direction at three points ①, ②, and ③.

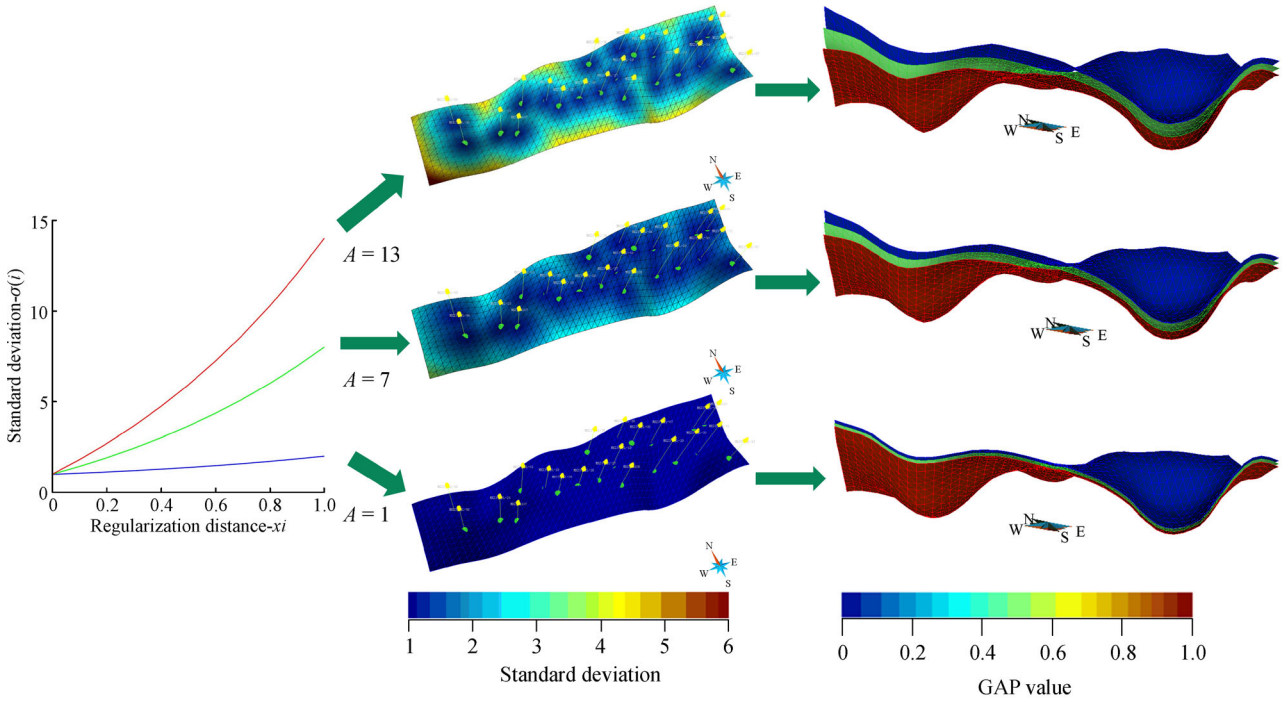

Fig. 4 Uncertainties distribution on subsurface with different distance factors and standard variation is 1.0 at the sample points. The left image shows the relationship between standard deviation variation with regularization distance, in which different distance factors are 1 (blue line), 7 (green line), and 13 (red line). The standard variation with different distance factors is shown in the middle image. The GAP values in green, brown, and blue in the right image are 0.1, 0.5, and 0.95, respectively, in which the distance factors are same to the middle images.

curvature and Gaussian curvature are discussed to characterize the impact of uncertainty on subsurface geometry.

With the variation of GAP values, the geometry of the buffer zone varies constantly. The normal vector describes the orientation of the local surface. It is meaningful to describe uncertainty by depicting the variation of normal vectors on a geological subsurface. We need to obtain the unit normal vectors $\vec{N}$ of each node. The unit normal vector on a certain node can be obtained by weighting and summing the normal vectors of the triangles neighboring the node. As shown in Fig. 5, the purple vectors are the unit normal vectors, and all normal vectors point to the same side of a surface.

The orientation variation of GAP isosurfaces can be characterized clearly by normal vectors. However, the curvature property in different tangential directions varies on a structural surface. Also, this type of anisotropic

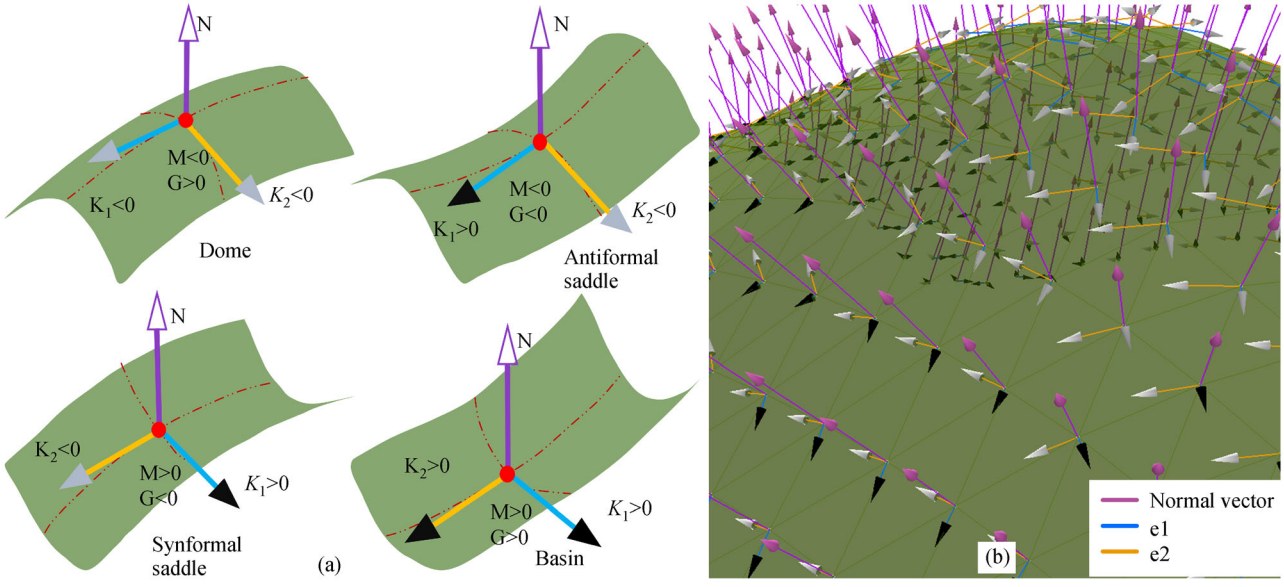

Fig. 5 Typical surface with their vectors and a local effect graph. (a) Vector parameters on four typical surfaces (After Lindsay et al., 2013). (b) Local effect graph of vector parametric system on a surface triangle network.

feature is a very important factor for quantifying uncertainties among GAP isosurfaces. Differential geometry provides an appropriate method for establishing the tangent vector system. Here, a pair of principal curvature vectors including the major principal curvature vector $\vec{e_1}$ and the minor principal curvature vector $\vec{e_2}$ are assigned on each node. The direction and the length of $\vec{e_1}$ are the major principal direction and the absolute value of the major principal curvature k_1, respectively. Likewise, the direction of $\vec{e_2}$ is the minor principal direction and the length of $\vec{e_2}$ is the absolute value of the minor principal curvature k_2. The two principal directions are always perpendicular to each other and correspond to the maximum and minimum normal curvature, respectively. Therefore, they are the most typical tangent vectors that can fully depict the anisotropy feature of the uncertainty of a geological subsurface. In this study, the principal curvature vectors are obtained based on the algorithm provided by Dong and Wang (2005) and visualized in the form of line features, as shown in Fig. 5(a). The length of the principal curvature vector line represents the magnitude of the absolute value of the principal curvature, and the vector arrows are assigned either black or gray color to distinguish values of positive and negative curvature, respectively (Fig. 5(b)).

Some scalar parameters including mean curvature and Gaussian curvature, which can describe the geometrical variation of GAP isosurfaces, are also discussed. These two parameters can be obtained from principal curvatures as follows:

$$M = \frac{(k_1 + k_2)}{2},\ G = k_1 \cdot k_2, \tag{2}$$

where k_1 and k_2 are two principal curvatures, and M, G are mean curvatures and Gaussian curvature, respectively.

Geometrically, mean curvature describes the average degree of curvature in all directions at a certain point, whereas Gaussian curvature reflects the total degree of curvature at a certain point. Figure 5(a) shows the positive and negative discriminant of Gaussian curvature and mean curvature of four typical surfaces. Obviously, the geometrical variation can be described by Gaussian curvature and mean curvature.

Although the curvature can describe geometrical feature of a point, the impact of neighboring points is not taken into consideration. Also, curvature magnitude is extremely uneven on some strongly undulating surfaces due to the high sensitivity of the curvature feature. Entropy reflects the degree of disorder at a local region around a certain point. A larger entropy value indicates that a larger amount of information can be provided. Entropy calculation weakens the negative influence of the curvature not being able to consider the larger neighborhood (Li et al., 2015). Therefore, curvature entropy represents variation of curvature and the complexity of a surface as well as reduces the sensitivity of curvature. Curvature and curvature entropy should be considered simultaneously in order to obtain a continuous and complete description of the geometrical variation.

Curvature entropy can be calculated as follows (Li et al., 2015):

$$H_i = -p_i \log_2 p_i - \sum_{j=1}^{m} p_j \log_2 p_j, \tag{3}$$

where p_i and p_j are probabilities of curvature at the ith and

*j*th nodes, respectively, and can be expressed as

$$p_i = \frac{K_i}{K_i + \sum_{j=1}^{m} K_j},\ p_j = \frac{K_j}{K_i + \sum_{j=1}^{m} K_j}, \quad (4)$$

where K_i and K_j are the absolute values of curvature of the *i*th and *j*th nodes, respectively, the *j*th node is adjacent to the *i*th node, and *m* is the number of nodes involved in the calculation. The variation of curvature and its corresponding entropy of the subsurface have the same tendency, as shown in Fig. 6. As the curvature entropy considers the large neighborhood of each node, compared to variation of curvature, variation of curvature entropy is more continuous and softer at local positions. Therefore, curvature entropy is appropriate for describing geometrical variation of geological surfaces.

2.4 Uncertainty visualization of vector-based parameters

Theoretically, many GAP isosurfaces simulated by the MC method can be obtained. Each point on every GAP isosurface has its own vector parameters. Therefore, a comparison of values of vector parameters is key to analyzing and understanding the uncertainties among GAP isosurfaces. Three types of uncertainties visualization methods are presented in Fig. 7.

Normal vectors of points on each GAP isosurface are drawn on the corresponding surfaces in the 'separated' method, as shown in the first row of Fig. 7. The different colors along the direction of the surface illustrate the GAP value of the surface. The uncertainty difference caused by different standard deviation values is illustrated by the distances among normal vectors of GAP isosurfaces. However, this type of method cannot reflect the difference of direction of normal vectors. Therefore, an approach termed the 'focused' method is also presented here, as shown in the second row of Fig. 7. The focused method puts the starting point of all normal vectors of each point of the GAP isosurface on the best-guess surface. When the GAP isosurfaces are not perturbed, all normal vectors overlap and show as a straight line. Otherwise, the variation of all normal vectors appears gradually in the form of fan. The 'stream line' method is a third approach for visualizing uncertainties among GAP isosurfaces. In this situation, all normal vectors at the same location are concatenated end-to-end into a streamline, as shown in the third row of Fig. 7. As in the 'focused' method, when the GAP isosurfaces are not perturbed, the streamline shows as a straight line. A symmetric curve with its symmetry center on the best-guess subsurface occurs when uncertainties exist among the GAP isosurfaces.

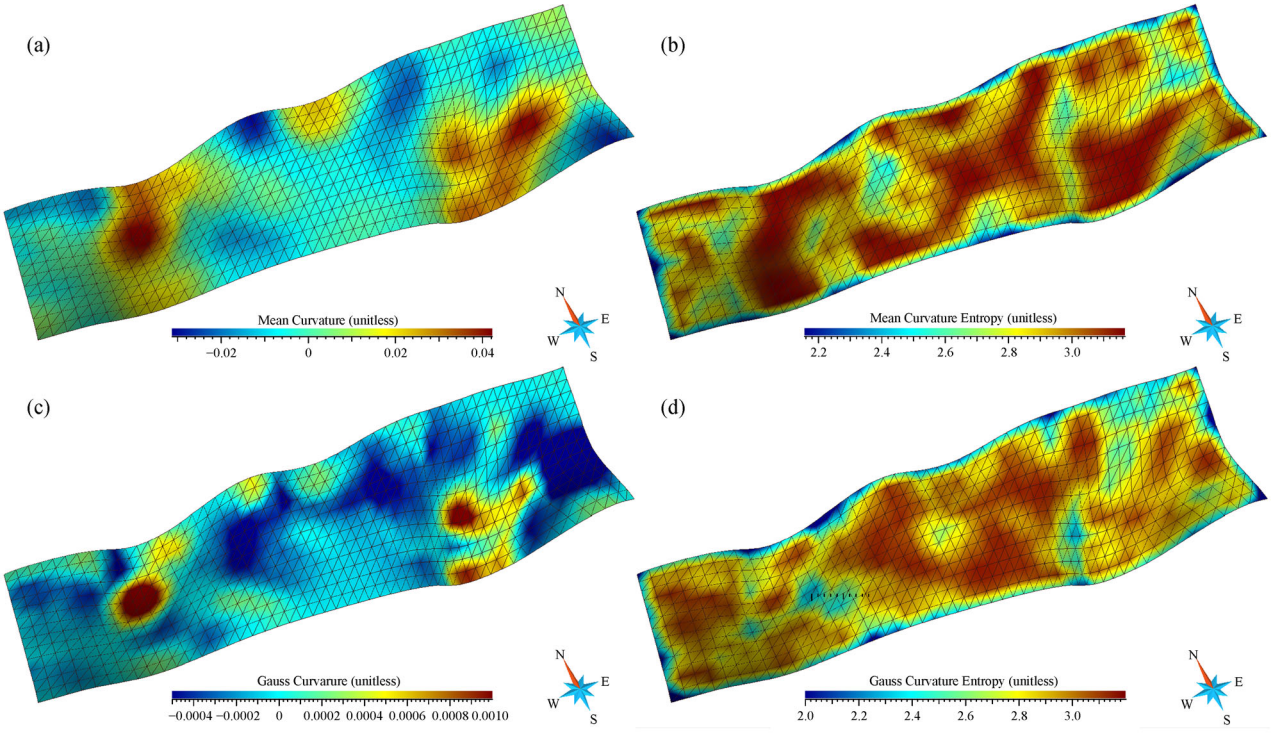

Fig. 6 Curvature and its entropy of subsurface. (a) and (b) are mean curvature and its entropy of subsurface, respectively; (c) and (d) are Gaussian curvature and its entropy of subsurface respectively.

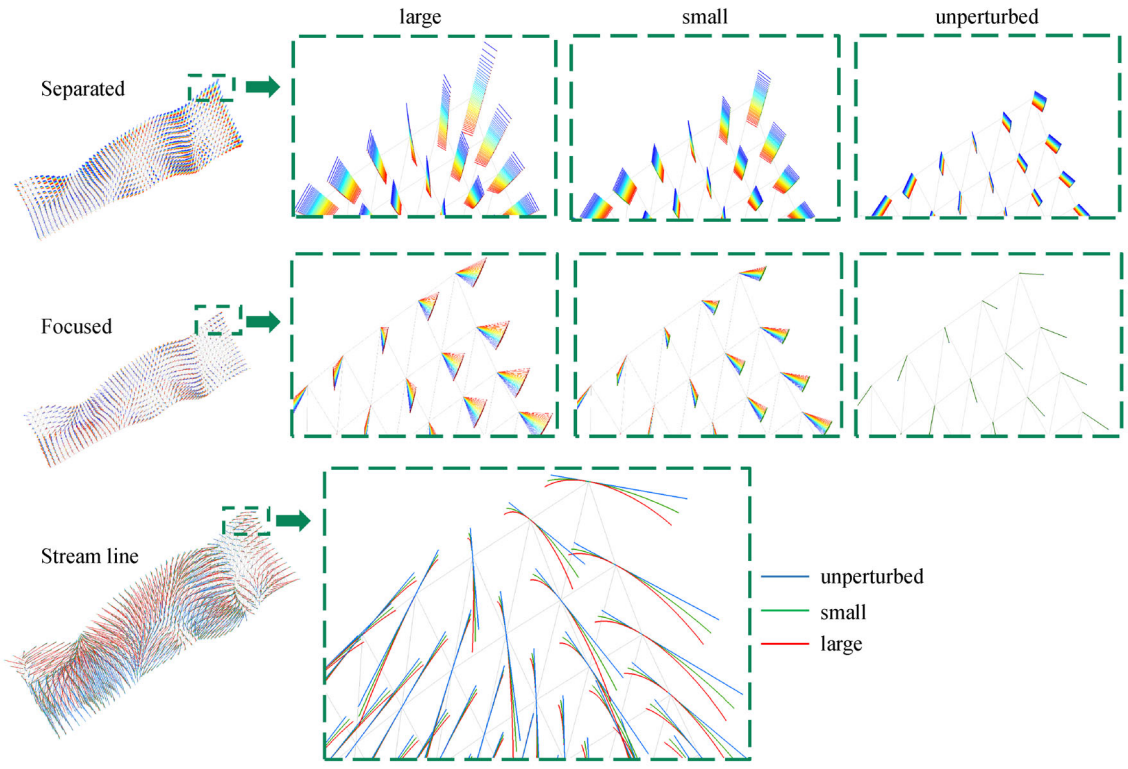

Fig. 7 Uncertainty visualization methods based on normal vector.

3 Results

3.1 3D fault surface model and model suite generation of study area

On the assumption that errors of fault position in borehole follow a normal distribution, the positions of each point on the interpolated fault surface were treated as the expected values with a standard deviation σ = 1.0 m, and the fault surface was supposed as being the best-guess surface and used as the initial surface for model suite construction. To discuss uncertainties variation, errors of the fault surface were calculated by Eq. (1) with different distance factors of 3, 5, 7, 9, 11, and 13. Hence, the probability density functions at each point on the fault surface could be calculated. For each distance factor, the GAP value of every point on the best-guess surface was calculated using the Monte Carlo simulation method described in Section 2. Therefore, each point has its own GAP distribution and isosurfaces, with 50 different GAP values being constructed.

3.2 Results visualization

Several model suites with different distance factors and standard deviation values were constructed. In each model suite, 50 fault interfaces were built with GOCAD®. The geometry difference among models with different distance factors is not very apparent, but the distance between the best-guess surface and other surfaces increases with distance factor increase.

In Fig. 7, normal vectors of every surface of each model suite are displayed with different methods. With the separated method, when standard deviation has the same value (such as σ = 1.0 m), the interval of normal vectors on every isosurface point increases with increase of the distance factor value. This reflects the same trend as illustrated in Fig. 4. With the focused method, when the distance factor equals 1.0, all normal vectors on every point of all isosurfaces show as a straight line. With increase of the distance factor value, the straight line spreads out into a fan. The normal vector of the best-guess surface is located in the middle of the fan, and the other normal vectors show an axial symmetric distribution. The fan area expands progressively with increase of the distance factor. With the stream line method, normal vectors on every point of all surfaces of each model suite distribute with point symmetry in the form of stream lines. However, the geometry of each stream line of each surface becomes different as the distance factor changes. The stream line displays as a straight line of the normal vector of the best-guess surface. The geometric shape displays as a type of hyperbolic curve, and the curvature increases with increase of the distance factor.

The principal curvature vector on every point of a surface has two main directions: $\vec{e_1}$ and $\vec{e_2}$. Here, the separated and focused methods are used to analyze uncertainty because the stream line method is not appropriate for visualizing the principal curvature vector. As shown in Fig. 8, the uncertainty among GAP isosurfaces of a model suite has the same trend. However, the principal curvature is very sensitive to the variation of geometrical shape. On the same point (marked with red circles in Fig. 8), the principal curvature may change with different distance factor values. Also, changes of the principal curvature illustrate the geometrical variations of GAP isosurfaces with different distance factor.

4 Discussion

4.1 Analysis with MDS

Although a vector parameter-based method of uncertainty visualization is proposed above, uncertainty cannot be quantitatively analyzed and visualized in detail. Nevertheless, the total diversity between the 50 GAP isosurfaces should be visualized by an appropriate method so that the inner uncertainty can be discussed from the macroscopic viewpoint. The multiple dimensional scaling (MDS) method (Borg and Groenen, 1997) is employed to map the high-dimensional samples into low-dimensional space based on the distance matrix, and relative distance is provided to present differences among samples. The MDS is a kind of distance-based metric approach to describe the dissimilarity between data. Note that the distance can be based on a norm, filters, wavelets, or any other relevant metric. Therefore, the MDS is a general method for calculating dissimilarity (Gregoire and Caers, 2015). A distance matrix D that describe the dissimilarity between GAP iso-surfaces and the best guess is obtained. Then, the D is translated into a configuration of points that defined is an n-dimensional Euclidean space $\Re$ (Gregoire and Caers, 2015). The Euclidean distances of the points in this space represent the dissimilarities of the objects involved. A coordinates matrix X that defines the position of each point in $\Re$ is the results of MDS. Therefore, the coordinates MDS plot represents the dissimilarity distance of the objects.

The total diversity of curvature and curvature entropy are visualized by the MDS algorithm provided by Caers (2011). In this study, Euclidean distance is used to characterize differences among GAP isosurfaces in the distance matrix. We mapped Gaussian curvature, mean curvature, their entropy values, normal vectors, and principle directions of the best-guess model and other models with different distance factor values and deviation values in using MDS plots (Fig. 9). The distance factor is set as 3, 5, 7, 9, 11, and 13, and the standard deviation values are 0.7, 1.0, 1.2, and 1.5.

In the images of each column in Fig. 9, when the standard deviation has the same value, the distribution of GAP isosurfaces spreads wider with increase of distance factor value. Except for Gaussian curvature and its entropy, all models with different GAP isosurfaces distribute as an axial symmetric distribution with the center at the best-guess model. Except that the different deviation value equals 1.2, the MDS plots of mean curvature with different deviation values distribute as a straight line. However, error perturbation of the subsurface cannot be displayed in the MDS plot. For the Gaussian curvature, normal vector, and mean curvature, when the deviation value is not 1.5, subsurface perturbation of error cannot be reflected effectively in the MDS plot. Although MDS plots of mean curvature entropy with different standard deviation distribute with an axial symmetric distribution, GAP

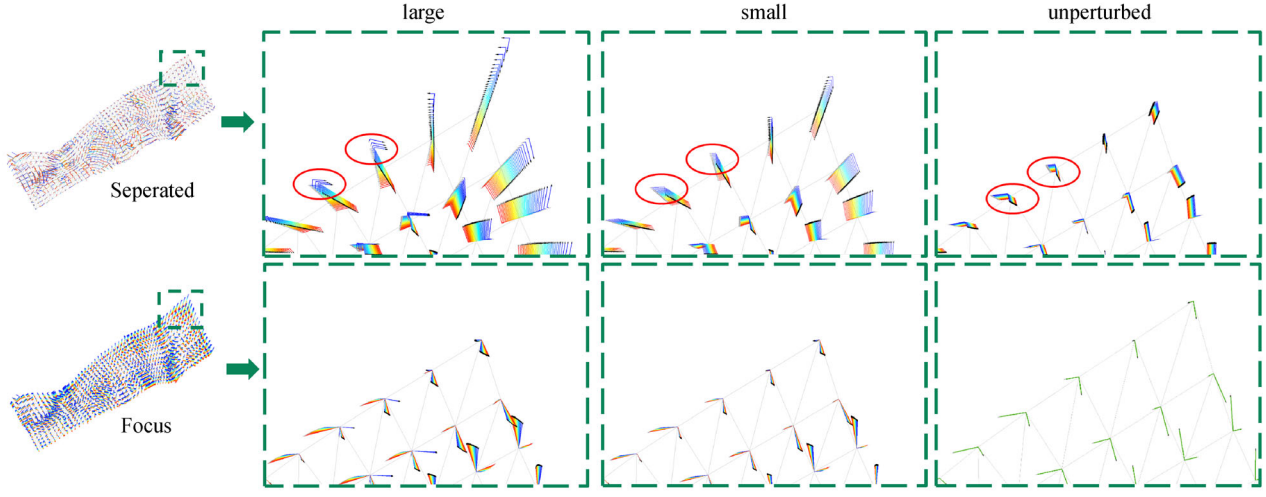

Fig. 8 Uncertainty visualization with principal curvature vectors. The red circle marked out the variation of principal curvature vectors change of the same point on different GAP iso-surface.

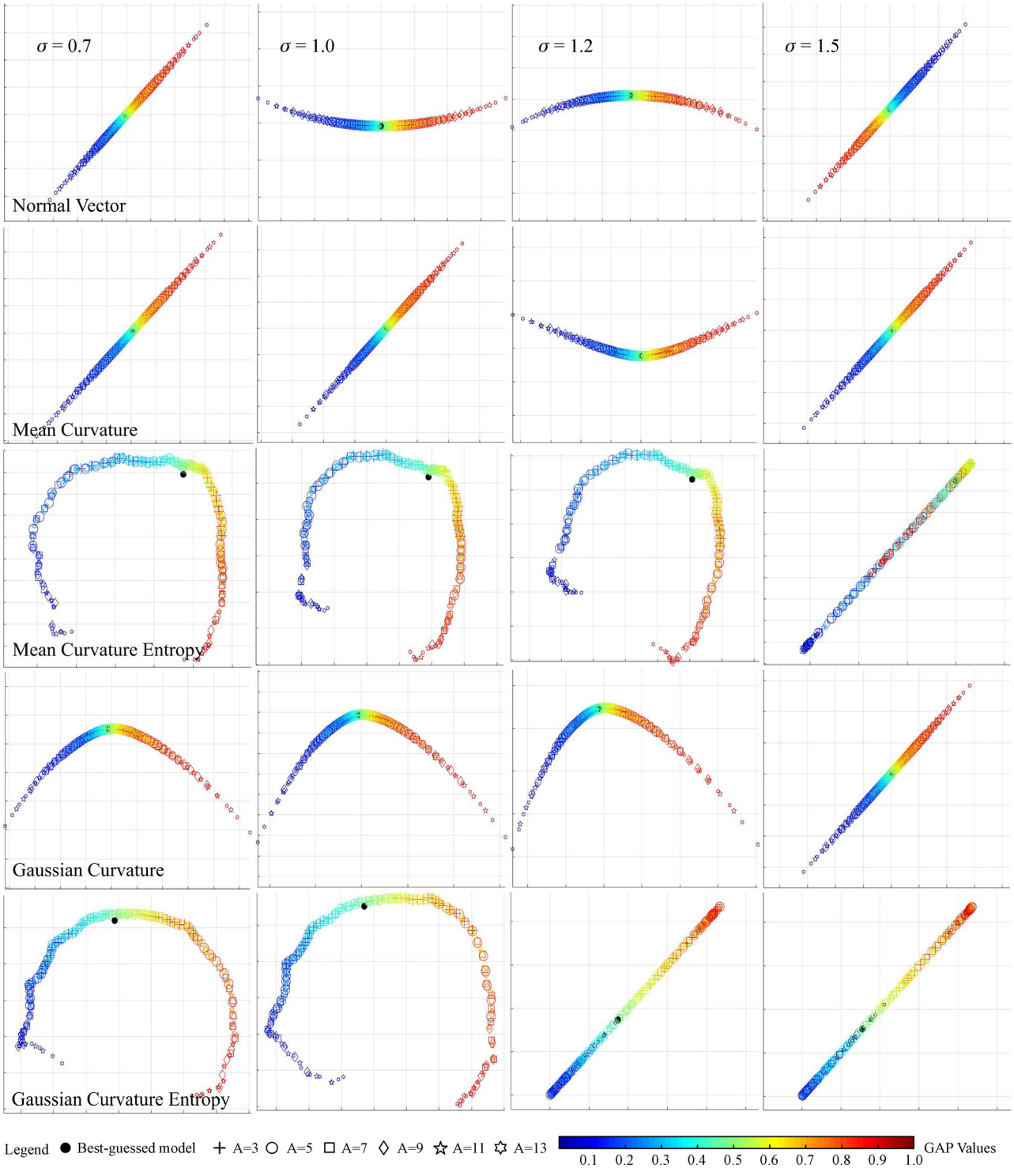

Fig. 9 MDS plots of results with different parameters. Four images with σ = 0.7, 1.0, 1.2, and 1.5 in each row are MDS plots of normal vector, mean curvature, mean curvature entropy, Gaussian curvature and Gaussian curvature entropy respectively. Images of each column are MDS plots of different parameters with the same standard deviation value. The dark cycle in the image is the best-guessed model. Other symbols represent models with different distance factors (A). Color bar in the legend is the scalar of GAP values,

isosurfaces of which values are larger than 0.5 are more concentrated. The MDS plots of Gaussian curvature entropy have an opposite trend compared to the mean curvature entropy. When the standard deviation value is smaller than 1.0, the tails of the MDS plots of Gaussian curvature entropy become sparser and more disordered with the increase of standard deviation. When the standard deviation value is larger than 1.0, the MDS plots of Gaussian curvature entropy distribute as a straight line. The distribution of the major and minor principal directions of all models appears similarly symmetric. However, when deviation value equals 1.5, except for the principal curvature vector, the MDS plots of all other parameters on different GAP isosurfaces distribute as a straight line, and the disturbance of GAP isosurfaces is not reflected effectively. When the distance factor is a constant, the distribution scope of GAP isosurfaces increases with standard deviation value increase in MDS plots, as shown in Fig. 10. For the mean curvature entropy and Gaussian curvature entropy, the tails of the GAP isosurfaces distribution in MDS plots have a different trend when the standard deviation value increases.

To explore the impact of different error existing in the GAP isosurfaces, one point was perturbed with different standard deviation values and the GAP isosurfaces were reconstructed. The standard deviation values on all sample points, except the perturbed point, are preset as 1.0, and the distance factor is 3.0. On the perturbed point, the standard deviation values are preset as 0.5, 1.0, and 1.5. When the standard deviation value increases from 0.15 to 1.5, the distribution scope of GAP isosufaces in MDS plots does not change obviously, as shown in Fig. 11. Also, for the mean curvature entropy and Gaussian curvature entropy, the tails of the GAP isosurfaces distribution have a different trend irrespective of what the standard deviation value is.

In the presented method, the distance factor and the standard deviation together determined the shape of the geological subsurface. When the standard deviation value is small, the mean curvature entropy and Gaussian curvature entropy are effective parameters for describing the uncertainty existing in geological subsurfaces caused by errors. The error perturbance of GAP isosurfaces can be reflected by the mean curvature entropy and Gaussian curvature entropy in MDS plots.

5 Conclusions

This study presented an uncertainty visualization method with vector-based parameters for the 3D geological subsurface. Under the premise of converting the 3D spatial error of the modeling data into the one-dimensional geological attribute probability distribution, the GAP isosurface suite is constructed. To analyze the response to different parameters, several GAP isosurface suites with different distance factors are constructed. The vector parameters, the curvature, and the curvature entropy of these equivalent probability surfaces are visualized, and the total diversity of these surfaces are expressed by the MDS method. The case study illustrated that the principal curvature vector is the most sensitive parameter among all

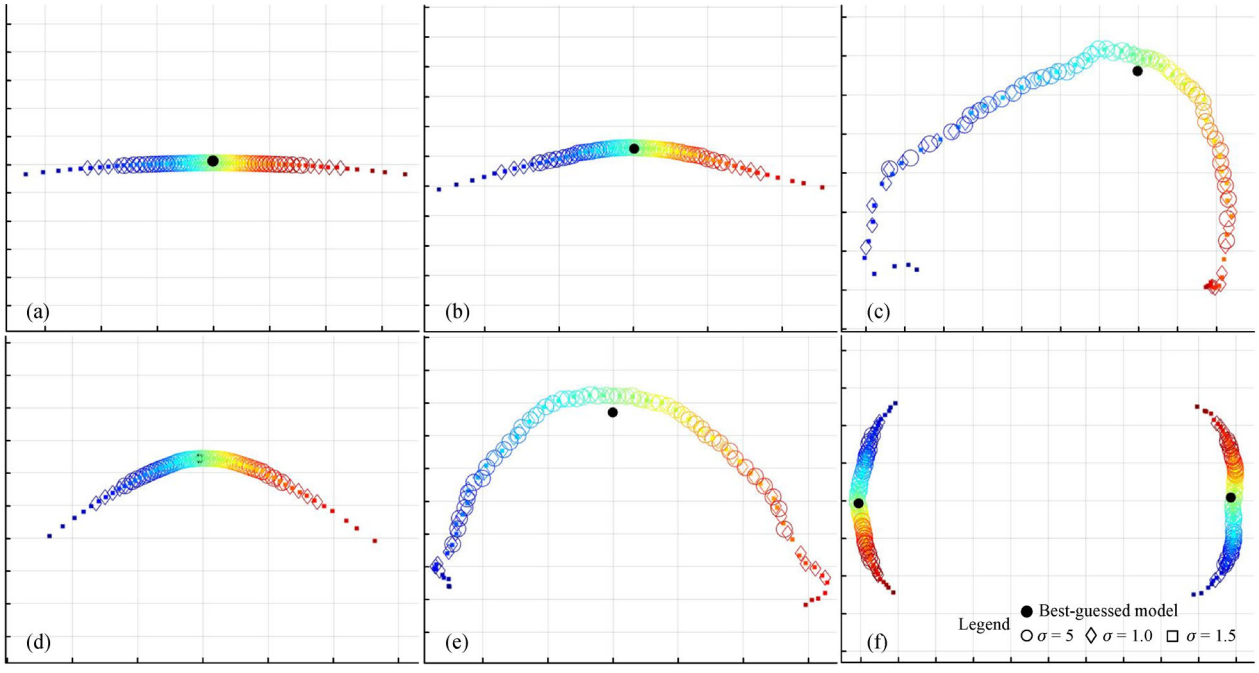

Fig. 10 MDS plots of GAP iso-surfaces with different standard deviation values when distance factor is 1.0. Images from (a) to (f) are different vector parameters of normal vector, mean curvature, mean curvature entropy, Gaussian curvature, Gaussian.

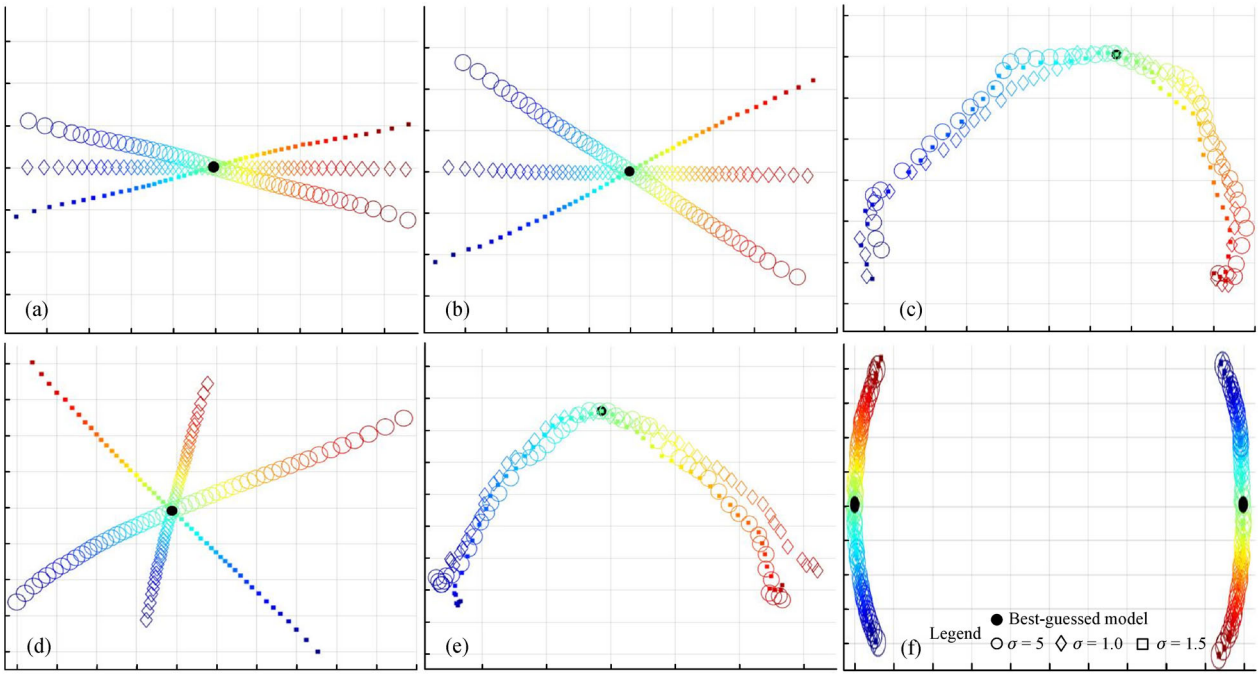

Fig. 11 MDS plots of GAP iso-surfaces with one perturbed point where distance factor is 3.0, standard deviations of the perturbed point are 0.5, 1.0, and 1.5 and other points are 1.0. Images from (a) to (f) are different vector parameters of normal vector, mean curvature, mean curvature entropy, Gaussian curvature, Gaussian curvature entropy, and the principal vector, respectively.

the parameters presented. The curvature and its entropy are appropriate for describing the anisotropy feature of uncertainty in a geological surface model. Compared to the scalar-based visualization methods, the visualization system presented is more appropriate for revealing the inner uncertainty of a 3D geological surface model.

In practice, a best-guess of geological structure is built by boreholes and cross-sections. According to the lithological types and characteristics of core samples, error distribution function and corresponding parameters at each contact point are preset. When the geological sub-surface like fault or weathered bedrock is near to or interacts with the bottom or top of metro structures, the sub-surface of the extreme depth has the maximum or minimum impact of metro construction. The variation of the curvature and its entropy of sub-surfaces reflects the difficulties of rock erosion. A suite of GAP model provides different models for calculating rock mechanics for metro constructions, and different probabilities for decision-making for metro design and construction method.

Acknowledgements This research was substantially supported by the National Natural Science Foundation of China Program (Grant Nos. 41472300 and 41772345), and Innovation Group Project of Southern Marine Science and Engineering Guangdong Laboratory (Zhuhai) (No. 311021003).

References

Bárdossy G, Fodor J (2004). Evaluation of Uncertainties and Risks in Geology-New Mathematical Approaches for Their Handling. New York: Springer Press

Bistacchi A, Massironi M, Dal Piaz G V, Dal Piaz G, Monopoli B, Schiavo A, Toffolon G (2008). 3D fold and fault reconstruction with an uncertainty model: an example from an Alpine tunnel case study. Comput Geosci, 34(4): 351–372

Bond C E (2015). Uncertainty in structural interpretation: lessons to be learnt. J Struct Geol, 74: 185–200

Bond C E, Gibbs A D, Shipton Z K, Jones S (2007). What do you think this is? “Conceptual uncertainty” in geoscience interpretation. GSA Today, 17(11): 4–10

Borg I, Groenen P (1997). Modern Multidimensional Scaling: Theory and Applications. New York: Springer

Caers J (2011). Modelling Uncertainty in the Earth Sciences. Chichester: Wiley-Blackwell

Calcagno P, Chilès J P, Courrioux G, Guillen A (2008). Geological modelling from field data and geological knowledge: part I. modelling method coupling 3D potential field interpolation and geological rules. Phys Earth Planet Inter, 171(1–4): 147–157

Caumon G, Collon-Drouaillet P, Le Carlier de Veslud C, Viseur S, Sausse J (2009). Surface-based 3D modeling of geological structures. Math Geosci, 41(8): 927–945

Chilès J P, Aug C, Guillen A, Lees T (2004) Modelling of geometry of geological units and its uncertainty in 3D from structural data: the potential-field method. In: Ore body Modelling and Strategic Mine Planning–Uncertainty and Risk Management Models

de Kemp E A, Schetselaar M E, Hillier J M, Lydon W J, Ransom W P (2016). Assessing the workflow for regional-scale 3D geologic modeling: an example from the Sullivan time horizon, Purcell Anticlinorium East Kootenay region, southeastern British Columbia.

Interpretation (Tulsa), 4(3): SM33–SM50

Dong C S, Wang G Z (2005). Curvature estimation on triangular mesh. J Zhejiang Univ Sci A, 6: 128–136

González-Garcia J, Jessell M (2016). A 3D geological model for the Ruiz-Tolima Volcanic Massif (Colombia): assessment of geological uncertainty using a stochastic approach based on Bézier curve design. Tectonophysics, 687: 139–157

Gregoire M, Caers J (2015). Multiple-Point Geostatistics: Stochastic Modeling with Training Images. New York: John Wiley & Sons

Guangdong Geological and Mineral Bureau (1989). 1:50,000 Regional geological survey report of Guangzhou area

Guillen A, Calcagno P, Courrioux G, Joly A, Ledru P (2008). Geological modeling from field data and geological knowledge: part II modelling validation using gravity and magnetic data inversion. Phys Earth Planet Inter, 171: 158–169

Hollister B E (2015). Visualizing multimodal uncertainty in ensemble vector fields. Dissertation for Doctor Degree. Santa Cruz: UC Santa Cruz

Hou W S, Cui C J, Yang L, Yang Q C, Clarke K (2019). Entropy-based weighting in one-dimensional multiple errors analysis of geological contacts to model geological structure. Math Geosci, 51(1): 29–51

Jessell W M, Ailleres L, de Kemp A E (2010). Towards an integrated inversion of geoscientific data: What price of geology? Tectonophys, 490(3-4): 294–306

Jones R R, McCaffrey J K, Wilson W R, Holdsworth E R (2004). Digital field data acquisition: towards increased quantification of uncertainty during geological mapping. Geol Soc Lond Spec Publ, 239(1): 43–56

Julio C, Caumon G, Ford M (2015). Sampling the uncertainty associated with segmented normal fault interpretation using a stochastic downscaling method. Tectonophysics, 639: 56–67

Lee K, Jung S, Choe J (2016). Ensemble smoother with clustered covariance for 3D channelized reservoirs with geological uncertainty. J Petrol Sci Eng, 145: 423–435

Li X, Li P, Zhu H (2013). Coal seam surface modeling and updating with multi-source data integration using Bayesian Geostatistics. Eng Geol, 164: 208–221

Li X Y, Zhang F, Zhu H J, Hu W, Li W (2015). A digital elevation model (DEM) clustering simplification algorithm based on curvature entropy and the Guassian mixture model. J Beijing Chem Tech (Natural Science Edition), 42(6): 103–108 (in Chinese)

Lindsay M D, Aillères L, Jessell M W, de Kemp E A, Betts P G (2012). Locating and quantifying geological uncertainty in three-dimensional models: analysis of the Gippsland Basin, southeastern Australia. Tectonophys, 546–547(3): 10–27

Lindsay M D, Jessell M W, Ailleres L, Perrouty S, de Kemp E, Betts P G (2013). Geodiversity: exploration of 3D geological model space. Tectonophys, 594: 27–37

Mann C J (1993). Uncertainty in geology. In: Davis C J, Herzfeld U C, eds. Computers in Geology-25 Years of Progress. New York: Oxford University Press, 241–254

Scheidt C, Jeong C, Mukerji T, Caers J (2015). Probabilistic falsification of prior geologic uncertainty with seismic amplitude data: application to a turbidite reservoir case. Geophysics, 80(5): M89–M12

Tacher L, Pomian-Srzednicki I, Parriaux A (2006). Geological uncertainties associated with 3-D subsurface models. Comput Geosci, 32(2): 212–221

Thore P, Shtuka A, Lecour M, Ait-Ettajer T, Cognot R (2002). Structural uncertainties: determination, management and applications. Geophysics, 67(3): 840–852

Turner A K, Kessler H (2015). Challenges with applying geological modelling for infrastructure design. In: Schaeben H, Tolosana Delgado R, van den Boogaart K G, van den Boogaart R, eds. Proceedings of IAMG 2015, Freiberg (Saxony), Germany, 2015, 49–58

Wellmann J F, Horowitz F G, Schill E, Regenauer-Lieb K (2010). Towards incorporating uncertainty of structural data in 3D geological inversion. Tectonophys, 490(3–4): 141–151

Wellmann F J, Regenauer-Lieb K (2012). Uncertainties have a meaning: information entropy as a quality measure for 3-D geological models. Tectonophys, 526–529: 207–216